

Phonon modes of monoclinic BiB₃O₆

A. Gössling^{*1}, T. Möller¹, W.-D. Stein¹, P. Becker³, L. Bohatý³, and M. Grüninger^{1,2}

¹ 2nd Physical Institute, University of Cologne, Zùlpicher Str. 77, 50937 Cologne, Germany

² 2nd Physical Institute, RWTH Aachen, Huyskensweg, 52056 Aachen, Germany

³ Institute of Crystallography, University of Cologne, Zùlpicher Str. 49b, 50674 Cologne, Germany

Received 23 May 2005, revised 7 July 2005, accepted 18 July 2005

Published online 21 July 2005

PACS 42.65.-k, 42.70.Mp, 63.20.Dj, 77.84.Fa

* Corresponding author: e-mail goessl@ph2.uni-koeln.de, Phone +49 221 470 3770, Fax +49 221 470 6708

We present a detailed study of the phonon modes of the monoclinic compound BiB₃O₆ based on polarized reflectivity measurements on single crystals.

The spectra are analysed by means of a generalized Drude–Lorentz model, which allows us to resolve the modes of A and B symmetry.

© 2005 WILEY-VCH Verlag GmbH & Co. KGaA, Weinheim

1 Introduction Bismuth triborate, BiB₃O₆, a polar, non-ferroelectric crystal has attracted interest in the last years due to its outstanding nonlinear optical properties [1–3]. The large optical nonlinearities open up a rich field of applications for frequency conversion of laser light via $\chi^{(2)}$ and $\chi^{(3)}$ processes, e.g. phase-matched second harmonic generation (SHG) or optical parametric oscillation (OPO) and stimulated Raman scattering (SRS).

The exceptional optical nonlinearities of BiB₃O₆ have been attributed to the bonds of the [BO₃] units and to a lone-pair electron at the Bi ion [4]. Detailed studies of the lattice dynamics are required for a quantitative description of these bonds. Infrared (IR) and Raman studies of the phonons are so far only available at room temperature [3, 5–8]. In particular, there is no polarization-dependent infrared study, but a polarization analysis is essential for an accurate determination of the phonon frequencies in monoclinic crystals [9]. In this letter we present a detailed investigation of the linear optical response of BiB₃O₆ in the phonon range for different polarizations at $T = 20$ K and 300 K. The data are analyzed in terms of a generalized Drude–Lorentz model, which allows us to obtain the frequency, the damping, the strength and the orientation of the dipole moment of each phonon mode.

2 Experimental Milky-colored, right-handed single crystals of BiB₃O₆ with dimensions of $15 \times 15 \times 4$ mm³ and $8 \times 8 \times 2$ mm³ were grown using the top seeded growth technique [8, 10]. The crystal structure with space group symmetry C2 (C_2^3) ($a = 7.116(2)$ Å, $b = 4.993(2)$ Å, $c = 6.508(3)$ Å, $\beta = 105.62(3)^\circ$) consists of sheets of cor-

ner-sharing [BO₃] and [BO₄] units in a ratio of 2:1. These sheets are separated by sheets of six-fold coordinated Bi [11]. We performed reflectivity measurements at $T = 20$ K and 300 K in the spectral range of 50–8000 cm⁻¹ at quasi-normal incidence. Using a Bruker IFS 66v/S Fourier-transform spectrometer the spectra were measured for different polarization angles on polished (010) and (100) surfaces of BiB₃O₆. As a reference we used an Au mirror. The variation of the polarization angle was realized by rotating the polarizer.

3 Phonon modes The factor group analysis [12] yields the following irreducible representations for the space group C2:

$$\Gamma_{\text{BiB}_3\text{O}_6} = \Gamma_{C_2^3} = 14A + 16B. \quad (1)$$

After subtraction of the three acoustic modes $A + 2B$, our group theoretical analysis predicts 13 A and 14 B optical phonon modes. Due to the lack of a center of inversion, A and B modes are active both in Raman [6, 7] and in IR spectroscopy. The linear dielectric response (without external magnetic field) of a monoclinic sample can be described by the tensor

$$\hat{\epsilon} = \begin{pmatrix} \epsilon_{xx} & 0 & \epsilon_{xz} \\ 0 & \epsilon_{yy} & 0 \\ \epsilon_{xz} & 0 & \epsilon_{zz} \end{pmatrix}. \quad (2)$$

Note, that we assume $\mathbf{y} \parallel \mathbf{b}$, $\mathbf{z} \parallel \mathbf{c}$, and $\mathbf{x} \perp \mathbf{c}$ lying in the \mathbf{ac} plane, where \mathbf{a} , \mathbf{b} , and \mathbf{c} are the crystallographic axes (see inset of Fig. 1a). In order to determine the phonon modes

© 2005 WILEY-VCH Verlag GmbH & Co. KGaA, Weinheim

we follow the procedure described in Ref. [9]. The tensor (2) can be decomposed into a scalar ε_b along the \mathbf{b} axis and a two-dimensional tensor $\hat{\varepsilon}_{ac}$ within the \mathbf{ac} plane. Since the \mathbf{b} axis is perpendicular to the \mathbf{ac} plane, the A-symmetry modes can be probed by measuring with the incident electric field \mathbf{E} parallel to the \mathbf{b} axis (e.g. on a (100) surface). Determining the B-symmetry modes requires the analysis of at least three polarization directions (with $\mathbf{E} \parallel \mathbf{ac}$ plane on a (010) surface) because the angle between the \mathbf{a} and the \mathbf{c} axis deviates from 90°. Reflectivity spectra at $T = 300$ K are shown for $\mathbf{E} \parallel \mathbf{ac}$ in Figs. 1a–c and for $\mathbf{E} \parallel \mathbf{b}$ in Fig. 1d. The phonons extend up to almost 1500 cm⁻¹ due to the small mass of the B ions.

The dispersion of the scalar ε_b is described by the sum of oscillators (Drude–Lorentz model), whereas the tensor $\hat{\varepsilon}_{ac}$ is described by a generalized Drude–Lorentz model:

$$\varepsilon_b(\omega) = \varepsilon_{yy} = \varepsilon_b^\infty + \sum_{i,A} \frac{\omega_{p,i}^2}{\omega_{0,i}^2 - \omega^2 - i\gamma_i\omega},$$

$$\hat{\varepsilon}_{ac}(\omega) = \begin{pmatrix} \varepsilon_{xx} & \varepsilon_{xz} \\ \varepsilon_{xz} & \varepsilon_{zz} \end{pmatrix} = \hat{\varepsilon}_{ac}^\infty + \sum_{i,B} \frac{\omega_{p,i}^2}{\omega_{0,i}^2 - \omega^2 - i\gamma_i\omega} \times \begin{pmatrix} \cos^2 \theta_i & \sin \theta_i \cos \theta_i \\ \sin \theta_i \cos \theta_i & \sin^2 \theta_i \end{pmatrix}. \quad (3)$$

Here, ε_b^∞ and $\hat{\varepsilon}_{ac}^\infty$ are the high-frequency dielectric constants, $\omega_{0,i}$ is the transverse frequency, $\omega_{p,i}$ the plasma frequency, γ_i the damping of the i -th oscillator, and θ_i (for the B modes) the angle between the dipole moment and the \mathbf{x} axis. Due to the low symmetry, the orientation of the principal axes of $\hat{\varepsilon}_{ac}$ depends on ω and is different for $\text{Re}\{\hat{\varepsilon}_{ac}\}$ and $\text{Im}\{\hat{\varepsilon}_{ac}\}$. The rotation angles ϕ_{Re} and ϕ_{Im} can be calculated by diagonalizing $\text{Re}\{\hat{\varepsilon}_{ac}\}$ and $\text{Im}\{\hat{\varepsilon}_{ac}\}$ by two different rotation matrices. An example for the relationship between ϕ_{Im} , ϕ_{Re} , and θ_i is shown in the inset of Fig. 1e. In the case of a strong oscillator (e.g. $\omega_0 = 1363$ cm⁻¹, see below), $\phi_{\text{Im}}(\omega_0)$ and θ_i are similar, but they may differ significantly for a weak mode.

The reflectance for $\mathbf{E} \parallel \mathbf{b}$ (R_b) and $\mathbf{E} \parallel \mathbf{ac}$ (R_{ac}) can be obtained by using the Fresnel equations for normal incidence [9]:

$$R_b = \left| (1 - \sqrt{\varepsilon_b}) \cdot (1 + \sqrt{\varepsilon_b})^{-1} \right|^2,$$

$$R_{ac}(\chi) = \left| \left((1 - \sqrt{\hat{\varepsilon}_{ac}}) \cdot (1 + \sqrt{\hat{\varepsilon}_{ac}})^{-1} \right) \begin{pmatrix} \cos \chi \\ \sin \chi \end{pmatrix} \right|^2. \quad (4)$$

In Eq. (4), χ denotes the angle between the polarization direction and the \mathbf{x} axis as shown in Fig. 1a. In order to take the square root of a tensor, $\hat{\varepsilon}_{ac}$ first has to be rotated to a diagonal form, then the square root has to be taken for each element, and finally the resulting tensor is rotated back to its original basis.

The scalar ε_b is determined by fitting the single spectrum R_b , while $\hat{\varepsilon}_{ac}$ is determined by fitting $R_{ac}(\chi)$ for three different values of χ simultaneously (we have measured $R_{ac}(\chi)$ for 14 different χ values). The fits yield an excellent description of the measured reflectivity. The fit param-

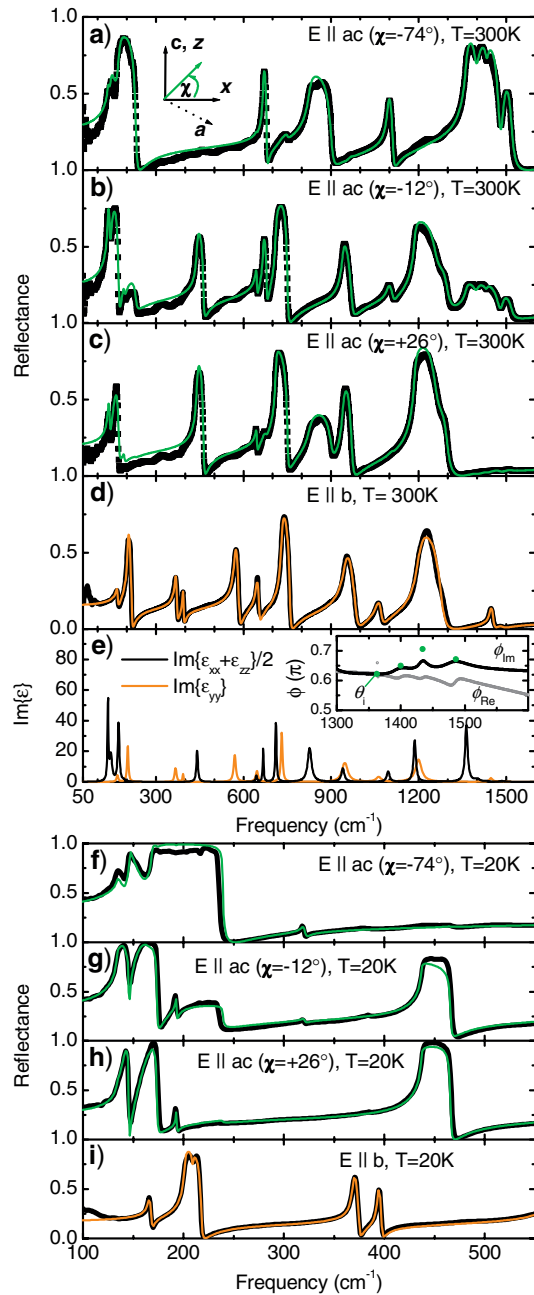


Figure 1 (online colour at: www.pss-rapid.com) **a)–c)** Reflectivity spectra of BiB₃O₆ at $T = 300$ K for $\mathbf{E} \parallel \mathbf{ac}$ plane at different polarization angles χ (black) and fits using Eq. (4) (grey). **d)** Reflectivity at $T = 300$ K for $\mathbf{E} \parallel \mathbf{b}$ (black), fit using Eq. (4). **e)** Components of $\text{Im}\{\hat{\varepsilon}\}$ for the fitted parameters; comparison of θ_i , ϕ_{Im} , and ϕ_{Re} (inset). **f)–h)** Reflectivity spectra of BiB₃O₆ at $T = 20$ K for $\mathbf{E} \parallel \mathbf{ac}$ plane at different polarization angles χ (black) and fits using Eq. (4) (grey). **i)** Reflectivity at $T = 20$ K for $\mathbf{E} \parallel \mathbf{b}$ (black), fit using Eq. (4).

eters are listed in Table 1, and Fig. 1e shows $\text{Im}\{\varepsilon_{yy}\}$ and $\text{Im}\{\varepsilon_{xx} + \varepsilon_{zz}\}/2$, which is independent of θ .

In case of $\mathbf{E} \parallel \mathbf{b}$, where 13 A modes are expected, we find 11 strong IR modes and a series of weaker features. Most of the latter can be interpreted as multi-phonon exci-

Table 1

Fit results for the reflectivity of BiB₃O₆ at $T = 300$ K using Eq. (4). Here, ω_0 is the transverse frequency, ω_p the plasma frequency, γ the damping, θ the angle between the dipole moment and the x axis (in case of the B modes), and $S = \omega_p^2/\omega_0^2$ denotes the oscillator strength. The high-frequency dielectric constants at $T = 300$ K are: $\epsilon_{xx}^\infty = 3.5$, $\epsilon_{yy}^\infty = 2.9$, $\epsilon_{zz}^\infty = 3.3$ and $\epsilon_{xz}^\infty = -0.3$. The four weak B modes at 1268, 1400, 1434, and 1486 cm^{-1} probably correspond to multi-phonon excitations.

B modes					A modes			
ω_0 (cm^{-1})	ω_p (cm^{-1})	γ (cm^{-1})	θ ($^\circ$)	S	ω_0 (cm^{-1})	ω_p (cm^{-1})	γ (cm^{-1})	S
136	236	3.9	151	3.021	168	71	7.0	0.179
146	215	9.4	132	2.185	202	164	5.5	0.659
172	291	6.5	89	2.862	367	151	7.0	0.169
190	50	8.3	33	0.069	393	93	4.4	0.056
441	333	6.0	18	0.570	570	305	9.2	0.286
644	173	5.8	175	0.073	646	208	9.4	0.104
667	328	3.7	131	0.241	731	396	6.6	0.293
711	514	4.8	15	0.523	947	522	23.0	0.304
826	753	15.6	77	0.831	1062	256	20.0	0.058
940	448	12.1	6	0.227	1199	668	25.6	0.310
1095	415	11.5	111	0.143	1448	208	12.3	0.021
1187	792	9.7	16	0.445	1484	129	30.3	0.008
1363	1028	10.5	112	0.568				
1268	156	49.7	19	0.015				
1400	314	21.4	117	0.050				
1434	101	12.9	127	0.005				
1486	169	19.4	121	0.013				

tations, e.g., a very weak feature at 272 cm^{-1} , which can be attributed to an overtone of the B mode at 136 cm^{-1} (note that $B \otimes B$ yields A symmetry). In order to determine which of the weak features corresponds to a fundamental phonon mode, it is helpful to compare our data with Raman results [6, 7]. In a recent room-temperature Raman study [6], 12 A modes have been observed. Ten of these modes are found both in the Raman and in the IR data (the transverse frequencies agree within a few wave numbers). Combined with the two additional Raman modes at 1294 and 1488 cm^{-1} and with the strongly IR-active mode at 1062 cm^{-1} , we end up with 13 A modes, as expected. The Raman peak at 1488 cm^{-1} corresponds to a weak IR feature (at 1484 cm^{-1}). However, the Raman mode at 1294 cm^{-1} [6] was neither observed in our IR data nor in the Raman data of Ref. [7]. Other features, which are weak in both spectroscopies, can be attributed to multi-phonon excitations (e.g. the peak at 272 cm^{-1} discussed above) or to a polarizer leakage (e.g. the Raman mode at 443 cm^{-1} [6] corresponds to a strongly IR-active B mode).

In case of the ac plane, each phonon mode shows a different orientation θ of the dipole moment. This produces complex patterns in $R_{ac}(\chi)$ which cannot be described by a simple Drude–Lorentz model. For the description of $R_{ac}(\chi)$ we used 17 oscillators (see Table 1), in contrast to the 14 B modes predicted. The use of four oscillators below 250 cm^{-1} is based on the 20 K data (see Figs. 1f–h). At high frequencies, the four modes at 1268, 1400, 1434, and 1486 cm^{-1} are very weak and show rather large

values of the damping γ . These four modes probably have to be attributed to multi-phonon excitations. Note that weak features may have a significant influence on the reflectivity if they are located on top of a *Reststrahlenband*. In case of the B modes the discrepancies between IR and Raman data [6, 7] are much larger than for the A modes because transverse and longitudinal modes mix for $E \parallel ac$. We have been able to determine the transverse eigenfrequencies and the orientation θ of the dipole moments by using the generalized Drude–Lorentz model (Eq. (3)). In order to determine all 14 B modes and to distinguish two-phonon excitations from the one-phonon modes, detailed lattice-dynamical calculations are required.

References

- [1] H. Hellwig et al., Solid State Commun. **109**, 249 (1999).
- [2] H. Hellwig et al., J. Appl. Phys. **88**, 240 (2000).
- [3] A. A. Kaminskii et al., Opt. Commun. **206**, 179 (2002).
- [4] D. Xue et al., phys. stat. sol. (a) **176**, R1 (1999).
- [5] H. R. Xia et al., J. Raman Spectrosc. **33**, 278 (2002).
- [6] X. Hu et al., J. Appl. Phys. **97**, 033501 (2005).
- [7] D. Kasproicz et al., Cryst. Res. Technol. **40**, 459 (2005).
- [8] P. Becker et al., Cryst. Res. Technol. **36**, 27 (2001).
- [9] A. B. Kuz'menko et al., Phys. Rev. B **63**, 094303 (2001).
A. B. Kuz'menko et al., J. Phys.: Condens. Matter **8**, 6199 (1996).
- [10] P. Becker et al., J. Cryst. Growth **203**, 149 (1999).
- [11] R. Fröhlich et al., Acta Cryst. C **40**, 343 (1984).
- [12] D. L. Rousseau et al., J. Raman Spectrosc. **10**, 253 (1981).